Available online at www.sciencedirect.com
ScienceDirect
Journal of Computational Physics 225 (2007) 714–729
JOURNAL OF COMPUTATIONAL PHYSICS
www.elsevier.com/locate/jcp

Using the method of weighted residuals to compute potentials of mean force

Eric C. Cyr *, Stephen D. Bond

University of Illinois at Urbana-Champaign, Department of Computer Science, Urbana, IL 61801, USA

Received 28 July 2006; received in revised form 19 December 2006; accepted 22 December 2006
Available online 10 January 2007

Abstract

We propose a general framework for approximating the potential of mean force (PMF) along a reaction coordinate in conformational space. This framework, based on the method of weighted residuals, can be viewed as a generalization of thermodynamic integration and direct histogram methods. Using weighted residuals allows for higher-order approximations to the PMF in the form of a global spectral method or a finite element method. In addition, the higher degree of continuity provided by spectral and higher-order elements makes weighted residual methods an attractive choice for use in tandem with biasing force methods. As an analysis tool, the weighted residuals framework provides a context for direct comparison of thermodynamic integration and histogram based methods. For validation of the new method, numerical experiments are performed on two systems: a simple double-well and alanine dipeptide in vacuum. Comparisons between the new weighted residual methods, thermodynamic integration, and WHAM are performed. When configuration space is perfectly sampled the high-order weighted residual methods are found to exhibit exponential convergence. For more realistic sampling, the weighted residual methods performed comparably to the other two. However, results suggest that spectral type methods are more robust with respect to parameter choices describing the solution space.
© 2007 Elsevier Inc. All rights reserved.

Keywords: Potential of mean force; Method of weighted residuals; Free energy; Thermodynamic integration; Histogram methods

1. Introduction

The potential of mean force (PMF) is one of the most important concepts in physical and biological chemistry [1]. It describes the change in free energy along a "reaction coordinate" and determines the strength and likelihood of association in molecular systems [2]. Estimating the change in free energy between two molecular conformations is a challenging task due to the high dimensionality of phase space and complex structure of the energy landscape [3].

A variety of techniques have been developed to approximate the PMF including umbrella sampling [4], weighted histograms [5], free energy perturbation [6,7], thermodynamic integration [7,8], steered molecular

* Corresponding author.
E-mail addresses: ericcyr@uiuc.edu (E.C. Cyr), sdbond@uiuc.edu (S.D. Bond).

0021-9991/$ - see front matter © 2007 Elsevier Inc. All rights reserved.
doi:10.1016/j.jcp.2006.12.015

dynamics [9] and adaptive biasing forces [10–13]. These methods sample configuration space using a sequence of (biased) equilibrium or nonequilibrium molecular dynamics or Monte Carlo simulations. The PMF is recovered using either the observed probability density or mean force.

In this paper we propose a novel framework for the approximation of the PMF along a reaction coordinate from configurations generated by molecular dynamics and Monte Carlo simulations. This framework, based on the method of weighted residuals, allows for the comparison of a wide class of existing free energy methods and provides a platform for deriving new methods.

Comparisons between free energy methods have been performed in the past. Both [14,15] found that thermodynamic integration (TI) was slightly superior to free energy perturbation (FEP). In a study comparing the use of the weighted histogram analysis method (WHAM), TI and FEP to compute solvation free energies, WHAM was found to perform better than TI and FEP [16]. Recently the adaptive biasing force (ABF) method was favorably compared to a method based on Jarzynski's identity [12].

The structure for the remainder of this paper is as follows. In Section 2, we define the potential of mean force in terms of the underlying probability density function. Direct histogram, thermodynamic integration and umbrella sampling methods are reviewed in Section 3. Weighted residuals methods are introduced in Section 3.4, where it is shown that direct histogram and thermodynamic integration methods are both weighted residuals methods. This framework is used to develop two new methods based on Chebyshev polynomials and spectral elements. Analytical results using a simple model problem indicate that the weighted residual methods are more accurate when conformational space is well sampled. To investigate sampling sensitivity, a sequence of numerical experiments are conducted in Section 4. Results indicate that the new weighted residual methods are competitive and more robust with respect to parameter choices.

2. Potential of mean force

The potential of mean force (PMF) is the free energy along a reaction coordinate (or path) in conformational space. The reaction coordinate, denoted by $\xi(x)$, is a function which maps atomic positions, x, to a continuous collection of states, $\xi(x)$. A specific state, ζ, is the set of atomic positions for which $\xi(x) = \zeta$. The reduced probability density function corresponding to the state ζ is given by

$$\rho_\xi(\zeta) = \int \delta(\xi(x) - \zeta)\rho(x,p)\,\mathrm{d}x\,\mathrm{d}p, \tag{1}$$

where x is the atomic positions, p is the momenta, and $\rho(x,p)$ is the probability density function associated with the ensemble. In this paper we assume conformations are sampled from the constant temperature or canonical ensemble,

$$\rho(x,p) = \frac{\mathrm{e}^{-\beta H(x,p)}}{\int \mathrm{e}^{-\beta H(x',p')}\,\mathrm{d}x'\,\mathrm{d}p'}.$$

Here $H(x,p)$ is the Hamiltonian of the system, the sum of the potential and kinetic energy terms, and $\beta = 1/k_\mathrm{B}T$, where k_B is the Boltzmann constant and T is temperature. The PMF, $A(\zeta)$, is defined in terms of the relative probability density at a state ζ by

$$A(\zeta) = -\frac{1}{\beta}\ln\left(\frac{\rho_\xi(\zeta)}{\rho_\xi(\zeta_0)}\right), \tag{2}$$

where ζ_0 is the reference state which can be chosen arbitrarily. Note that the PMF is defined up to an additive constant depending on the reference state. For a finite range of states, $[\zeta_\mathrm{a}, \zeta_\mathrm{b}]$, the reference state is often set to ζ_a in which case the resulting PMF at ζ_b is the change in free energy between states ζ_a and ζ_b.

The mean force can be written as an ensemble average using the derivative of the PMF (see [12,13]). Differentiating Eq. (2) with respect to ζ results in

$$\frac{\mathrm{d}A(\zeta)}{\mathrm{d}\zeta} = \left\langle \frac{\partial H}{\partial \zeta} \right\rangle_\zeta = -\langle F_\xi \rangle_\zeta = -\frac{\int F_\xi(x,p)\delta(\xi(x)-\zeta)\rho(x,p)\,\mathrm{d}x\,\mathrm{d}p}{\int \delta(\xi(x)-\zeta)\rho(x,p)\,\mathrm{d}x\,\mathrm{d}p}, \tag{3}$$

where $\langle\cdot\rangle_\zeta$ denotes the average at $\xi(x) = \zeta$ [12,13]. The average $\langle F_\xi\rangle_\zeta$ is the mean force acting in the direction of the reaction coordinate. Here, $F_\xi(x,p)$ is a function of atomic positions and momenta. The analytical form used in this paper is

$$F_\xi(x,p) = -\frac{2}{\beta}\frac{\nabla\xi(x)^{\mathrm{T}}M^{-1}\xi''(x)M^{-1}\nabla\xi(x)}{Z_\xi(x)^2} - \frac{\nabla U(x)^{\mathrm{T}}M^{-1}\nabla\xi(x)}{Z_\xi(x)} + \frac{p^{\mathrm{T}}M^{-1}\xi''(x)M^{-1}p}{Z_\xi(x)}, \tag{4}$$

where M is the mass matrix, U is the potential energy and $Z_\xi = \nabla\xi^{\mathrm{T}}M^{-1}\nabla\xi$. The derivation of Eq. (4) can be found in [11]. Additional forms can also be found in [17,10], however, they are more cumbersome then Eq. (4) because they require a coordinate system orthogonal to ξ to be defined. A convenient representation of the mean force is the ratio of two ensemble averages,

$$\langle F_\xi\rangle_\zeta = \frac{\overline{F}_\xi(\zeta)}{\rho_\xi(\zeta)}. \tag{5}$$

Here, $\overline{F}_\xi(\zeta)$, is defined as the numerator of Eq. (3)

$$\overline{F}_\xi(\zeta) = \int F_\xi(x,p)\delta(\xi(x)-\zeta)\rho(x,p)\,\mathrm{d}x\,\mathrm{d}p.$$

3. Numerical methods

In this section we present numerical methods for approximating the PMF. We start by reviewing existing direct histogram and thermodynamic integration (TI) methods before introducing the weighted residuals method. Using the weighted residuals framework we show that the direct histogram and TI methods are similar in that they both treat the approximation to the PMF as a linear combination of basis functions along the reaction coordinate

$$A(\zeta) \approx \sum_{i=1}^{N} A_i\phi_i(\zeta).$$

The methods only differ in the choice of basis functions, ϕ_i, and formula for computing the coefficients, A_i. Each coefficient is a single degree of freedom describing the approximation, in this case the approximation has N degrees of freedom (DOF). To illustrate the flexibility of weighted residuals, we apply two new methods based on Chebyshev polynomials and spectral elements.

Without sufficient sampling of conformational space, none of the methods described in this paper can accurately reconstruct the PMF. In regions where $\rho_\xi(\zeta)$ is small, the sampling will be poor due to high potential barriers. Effective removal of these barriers can be difficult since it generally requires knowledge of the underlying PMF. One biasing method, known as umbrella sampling, uses a restraining potential to increase sampling in a region of interest. In Section 3.3, we review umbrella sampling and the weighted histogram analysis method (WHAM) for combining data from a sequence of biased simulations.

3.1. Direct histogram method

The direct method calculates the probability distribution simply by building a histogram using binning. Binning requires breaking up the reaction coordinate into intervals or bins and then counting the number of times a molecular dynamics (MD) or Monte Carlo (MC) simulation reaches each bin. This gives a histogram from which a piecewise-constant representation of the probability density function $\rho_\xi(\zeta)$ can be found. The coefficients in this expansion are calculated by

$$P_i = \frac{1}{\Delta}\int \phi_i(\xi(x))\rho(x,p)\,\mathrm{d}x\,\mathrm{d}p = \frac{1}{\Delta}\int_{-\Delta/2}^{\Delta/2}\rho_\xi(\zeta_i+\zeta)\,\mathrm{d}\zeta, \tag{6}$$

where ϕ_i is the unit constant basis function with support over the bin defined by the interval $\zeta_i \pm \Delta/2$. The approximation to $\rho_\xi(\zeta)$ is written

$$\hat{\rho}_\xi(\zeta) = \sum_{i=1}^{N} P_i \phi_i(\zeta).$$

Note in the limit as $\Delta \to 0$ the approximation $\hat{\rho}_\xi(\zeta) \to \rho_\xi(\zeta)$. To find the PMF, the approximate probability density function, $\hat{\rho}_\xi(\zeta)$, is inserted into Eq. (2) resulting in

$$A(\zeta) \approx -\frac{1}{\beta} \ln\left(\sum_{i=0}^{N} \frac{P_i}{P_0} \phi_i(\zeta)\right) = \sum_{i=0}^{N} -\frac{1}{\beta} \ln\left(\frac{P_i}{P_0}\right) \phi_i(\zeta) = \sum_{i=0}^{N} A_i \phi_i(\zeta).$$

The summation commutes with the logarithm only in the case that ϕ_i is piecewise-constant. This would not be possible if ϕ_i were a higher-order polynomial.

There are two forms of error arising from this approximation, statistical and truncation error. Statistical error comes from using a finite sample size to approximate an average. This error decreases as Δ increases. The truncation (or systematic) error is a result of approximating a delta function with $\frac{1}{\Delta}\phi_i$. To see this, consider Eq. (6). The coefficient P_i is also an approximation of $\rho_\xi(\zeta_i)$, where P_i and $\rho_\xi(\zeta_i)$ can be written as the ensemble average of $\frac{1}{\Delta}\phi_i$ and δ respectively. They are equivalent in the limit as $\Delta \to 0$; however, for nonzero Δ, a truncation error is made. Therefore the truncation error decreases as Δ decreases, which is in opposition to the statistical error. In the absence of statistical error, the total error will be equal to the error from a piecewise-constant approximation of the PMF. A complete discussion of these errors and how to balance the two can be found in [18].

3.2. Thermodynamic integration

Thermodynamic integration (TI) relies on Eq. (3) to compute the mean force. Once computed, the mean force is integrated along the reaction coordinate to recover the PMF

$$A(\zeta) = -\int_{\zeta_0}^{\zeta} \langle F_\xi \rangle_\zeta \, \mathrm{d}\zeta.$$

$\langle F_\xi \rangle_\zeta$ can be calculated from a constrained MD or MC simulation [19]; however, doing so suffers from problems due to non-ergodic sampling. Regions normally accessible may become blocked by high potentials perpendicular to the reaction coordinate. Consequently the configuration space is not adequately sampled in finite simulation time [13].

A second option for computing $\langle F_\xi \rangle_\zeta$ is to use an unconstrained simulation in which the system is allowed to move freely, both in the direction of the reaction coordinate and in perpendicular directions. In this paper TI is assumed to be unconstrained unless otherwise stated. From an implementation perspective TI uses binning similarly to the direct method. The reaction coordinate is broken up into bins and, over the course of an MD or MC simulation, values of $F_\xi(x,p)$ are recorded in each bin. In post processing, the bin averages are computed yielding an approximation of $\langle F_\xi \rangle_\zeta$. Similar to the direct method, the mean force calculated by TI yields a piecewise-constant approximation to $\langle F_\xi \rangle_\zeta$. The coefficients in this expansion are

$$F_i = \frac{\int_{-\Delta/2}^{\Delta/2} \overline{F}_\xi(\zeta_i + \zeta) \, \mathrm{d}\zeta}{\int_{-\Delta/2}^{\Delta/2} \rho_\xi(\zeta_i + \zeta) \, \mathrm{d}\zeta}. \tag{7}$$

In terms of ϕ_i, a unit constant basis function with support over the bin defined by the interval $\zeta_i \pm \Delta/2$, the approximation of $\langle F_\xi \rangle_\zeta$ at any value of the reaction coordinate is written as

$$\langle F_\xi \rangle_\zeta \approx \sum_{i=1}^{N} F_i \phi_i(\zeta).$$

Integrating results in

$$A(\zeta) \approx -\int_{\zeta_0}^{\zeta} \sum_{i=1}^{N} F_i \phi_i(\zeta') \, \mathrm{d}\zeta' = -\sum_{i=1}^{N} F_i \int_{\zeta_0}^{\zeta} \phi_i(\zeta') \, \mathrm{d}\zeta', \tag{8}$$

which implies that TI provides a piecewise-linear approximation of the PMF. The coefficients suffer from the same type of statistical and truncation error as the coefficients for the direct method. For perfect sampling (no statistical error) the error in the TI approximation will be equal to the error from a piecewise-linear approximation of the PMF. For this reason, if the PMF is smooth and the bin sizes are the same, the TI approximation will be better then the direct histogram approximation in the absence of statistical error.

Recently Darve et al. [10–12] proposed a TI method that uses the most recent estimate of the PMF to bias the simulation. This method is known as the adaptive biasing force (ABF) method. Continuously updating the biasing potential with the best estimate of the PMF allows for eventual convergence to uniform sampling along the reaction coordinate, which leads to better sampling and faster convergence to the PMF. A description of an implementation of ABF and its details can be found in [13].

3.3. Umbrella sampling

The problem of poor sampling in unlikely regions of configuration space is present in both TI and the direct method. One way to alleviate this problem is through umbrella sampling, originally described in [4]. The idea is to run several simulations/trajectories with sampling that is restricted to a small portion of the reaction coordinate using a (typically quadratic) restraint potential. Ensemble averages calculated in separate trajectories can be recombined to give the desired average (see [4,20]). It is also possible to reduce barriers along the reaction coordinate by applying a bias that is the negative of an estimate of the PMF. The removal of this bias is the same as for the restraint potentials.

When calculating the PMF with the TI method, the restraint potentials allow adequate sampling along the reaction coordinate over the domain of interest. Since the restraint potential depends only on the reaction coordinate, the sampling perpendicular to the reaction coordinate is not changed by the bias. Therefore, the average $\langle F_\xi \rangle_\zeta$ is unaffected by the bias and no re-weighting is required when recombining the samples.

For direct methods, the effects of the biasing potential must be removed from the resulting biased histogram. One of the most popular methods for bias removal is the weighted histogram analysis method (WHAM) [5], which employs a specific choice of weights to combine the averages. Briefly, if $\rho^i_\xi(\zeta)$ is an average calculated from the ith of T trajectories then $\rho_\xi(\zeta)$ can be calculated as

$$\rho_\xi(\zeta) = \sum_{i=1}^{\mathrm{T}} w_i(\zeta)\rho^i_\xi(\zeta), \quad \text{where } \sum_{i=1}^{\mathrm{T}} w_i(\zeta) = 1 \quad \forall\zeta.$$

The weights are chosen to minimize the variance in $\rho_\xi(\zeta)$. For more details, see [21,22].

3.4. Method of weighted residuals

The method of weighted residuals is a technique used to find approximate solutions to ordinary and partial differential equations of the form

$$Lu(x) = f(x) \quad \text{for } x \in \Omega, \tag{9}$$

where L is a differential operator and Ω is the domain of the problem. The approximate solution, $\hat{u}$, is represented as a linear combination of N basis functions ϕ_i whose span forms the trial space. The coefficients are determined by forcing the residual, $r(x) = L\hat{u}(x) - f(x)$, to be orthogonal to a test space spanned by N basis functions ψ_j. Enforcing orthogonality yields a set of N equations to be solved for N unknown coefficients

$$\int_\Omega \psi_j(x) r(x) w(x)\,\mathrm{d}x = 0 \quad \text{for } j = 1, \ldots, N,$$

where $w(x)$ is a strictly positive weight function. In the case that L is a linear operator, the resulting system of equations will also be linear.

Different choices for the basis functions ϕ_i and ψ_j result in different types of methods. Galerkin methods use the same trial and test space with $\phi_i = \psi_i$. Basis functions with global support yield global spectral methods, while a locally supported basis results in a finite element method. Further choices are $\psi_j = \delta$, which results in a collocation method and $\psi_j = 1$ on an element, which gives a finite volume method. The method of least

squares is also a weighted residual method with $\psi_j = \partial r/\partial u_j$, where u_i are the unknown trial space coefficients [23].

The weighted residuals approximation to the PMF can be found using the residual defined by Eq. (3). Using the uniform weight function, $w(\zeta) = 1$, and the test functions $\{\psi_i\}_{i=1}^N$ gives the N equations

$$\int_{\zeta_0}^{\zeta_f} \left(\frac{\partial A}{\partial \zeta} + \langle F_\xi \rangle_\zeta\right)\psi_j(\zeta)\,\mathrm{d}\zeta = 0 \quad \text{for } j = 1,\ldots,N.$$

A difficulty of this formulation is that to integrate $\langle F_\xi\rangle_\zeta\psi_i(\zeta)$ requires $\langle F_\xi\rangle_\zeta$ to be evaluated at quadrature points. Each evaluation is subject to both truncation and statistical error. This problem can be avoided if the weight function is chosen to be $w(\zeta) = \rho_\xi(\zeta)$, which results in the new set of equations

$$\int_{\zeta_0}^{\zeta_f} \left(\frac{\partial A}{\partial \zeta} + \langle F_\xi \rangle_\zeta\right)\psi_j(\zeta)\rho_\xi(\zeta)\,\mathrm{d}\zeta = 0 \quad \text{for } j = 1,\ldots,N. \tag{10}$$

Substituting the trial basis functions $\{\phi_i\}_{i=1}^N$ and simplifying Eq. (10) by applying Eq. (5) gives

$$\begin{aligned}
&\int_{\zeta_0}^{\zeta_f} \left(\frac{\mathrm{d}A}{\mathrm{d}\zeta} + \langle F_\xi \rangle_\zeta\right)\psi_j(\zeta)\rho_\xi(\zeta)\,\mathrm{d}\zeta = 0\\
&\quad\Rightarrow \int_{\zeta_0}^{\zeta_f} \frac{\mathrm{d}A}{\mathrm{d}\zeta}\psi_j(\zeta)\rho_\xi(\zeta)\,\mathrm{d}\zeta = -\int_{\zeta_0}^{\zeta_f} \langle F_\xi\rangle_\zeta\psi_j(\zeta)\rho_\xi(\zeta)\,\mathrm{d}\zeta\\
&\quad\Rightarrow \sum_{i=1}^N A_i \int_{\zeta_0}^{\zeta_f} \phi_i'(\zeta)\psi_j(\zeta)\rho_\xi(\zeta)\,\mathrm{d}\zeta = -\int_{\zeta_0}^{\zeta_f} \overline{F}_\xi(\zeta)\psi_j(\zeta)\,\mathrm{d}\zeta.
\end{aligned}$$

Notice the integrals in the last expression are ensemble averages. This further simplifies the system (assuming ϕ_i and ψ_j have support only on $[\zeta_0, \zeta_f]$) to give

$$\sum_{i=1}^N A_i\langle \phi_i'(\xi(x))\psi_j(\xi(x))\rangle = -\langle F_\xi(x,p)\psi_j(\xi(x))\rangle \quad \text{for } j = 1,\ldots,N, \tag{11}$$

where $\langle\cdot\rangle$ denotes the ensemble average over all of configuration space.

With an appropriate choice of basis functions it is possible to derive the TI method from the weighted residual framework. Define a grid such that $\zeta_i = \zeta_0 + \left(i - \frac{1}{2}\right)\Delta$ for $i = 1,\ldots,N$, where $\zeta_N + \Delta/2 = \zeta_f$. Now define the derivative of the basis function ϕ_i to be 1 on the interval $\zeta_i \pm \Delta/2$ and zero otherwise. Note these basis functions are the same as the basis functions used to approximate $A(\zeta)$ in TI (see Eq. (8)). They will make up the trial space in a weighted residual method. Using a least squares approach the test space will be spanned by ϕ_j'. Substituting the ϕ_j' for ψ_j in Eq. (11) results in

$$\begin{aligned}
&\sum_{i=1}^N A_i\langle \phi_i'(\xi(x))\phi_j'(\xi(x))\rangle = -\langle F_\xi(x,p)\phi_j'(\xi(x))\rangle\\
&\quad\Rightarrow A_j\langle \phi_j'(\xi(x))\phi_j'(\xi(x))\rangle = -\langle F_\xi(x,p)\phi_j'(\xi(x))\rangle\\
&\quad\Rightarrow A_j = -\frac{\langle F_\xi(x,p)\phi_j'(\xi(x))\rangle}{\langle \phi_j'(\xi(x))\phi_j'(\xi(x))\rangle} = -\frac{\int_{-\Delta/2}^{\Delta/2} \overline{F}_\xi(\zeta_j+\zeta)\,\mathrm{d}\zeta}{\int_{-\Delta/2}^{\Delta/2} \rho_\xi(\zeta_j+\zeta)\,\mathrm{d}\zeta} = -F_j
\end{aligned}$$

for $j = 1,\ldots,N$. The last step holds because the function ϕ_j' has support only on the interval $\zeta_i \pm \Delta/2$. Notice the coefficients A_j are the negatives of the F_i coefficients used by TI in Eq. (7). Hence, the weighted residuals method with a piecewise-linear trial space and a piecewise-constant test space is the same as TI.

A similar argument can made for the equivalence of the direct method and the weighted residual method, though the proof is more complex. If the reaction coordinate is aperiodic, then piecewise-constant basis functions for the trial space and piecewise-linear basis for the test space yields the direct method. For periodic systems, the direct method corresponds to a piecewise-constant trial space; however, the test space is not as simple. For more details and derivations, see Section A.1 of the Appendix. A summary of the spaces used by the direct method and TI is found in Fig. 1.

Both TI and the direct method correspond to low-order finite element methods. The systematic error of these methods can be decreased by increasing the number of intervals in the approximation, this process is referred to as *h*-refinement and yields algebraic convergence. It is possible when using Eq. (10) to use high-order finite elements so-called spectral element methods (SEM) or even global spectral methods (GSM). High-order approximations have greater smoothness and can also take advantage of the exponential convergence coming from increasing the order of the approximation, referred to as *p*-refinement. Hybrid methods that use both forms of refinement are possible, SEM is particularly well suited to this approach [23,24].

As an example, consider the double well potential

$$U(x,y) = 2(y - x^3 + x)^2 + \frac{1}{4}x^4 + \mathrm{e}^{-x^2}. \tag{12}$$

If we let the reaction coordinate be defined as $\xi(x,y) = x$, then the PMF up to an additive constant, C, is

$$A(x) = \frac{1}{4}x^4 + \mathrm{e}^{-x^2} + C. \tag{13}$$

Under the assumption of perfect sampling (i.e. no statistical error), the application of Eq. (10) on the interval $[-1.5, 1.5]$ leads to the convergence in L^2 with respect to the degrees of freedom seen in Fig. 2. Here the GSM uses Chebyshev polynomials, refining solely in *p*, resulting in rapid exponential convergence. The steps in the curve are due to the even-degree of the exact solution since the addition of odd-degree basis functions does not improve the approximation. The SEM shows similar rapid convergence due to *p*-refinement. Here the number of elements is held fixed at 50 while each element is refined in *p*. Finally, TI uses fixed-degree piecewise-linear elements combined with pure *h*-refinement.

In addition to the rapid theoretical convergence and greater smoothness of higher-order approximations, *p*-refinement also reduces the statistical error associated with small bin sizes. For a SEM, the bin (or element size) can remain fixed while the degree is increased. Alternatively, if a GSM is used there will be no sampling

Method	Trial Space	Test Space
TI	Piecewise Linear	Piecewise Constant
Direct Method	Piecewise Constant	Piecewise Linear*

*For aperiodic reaction coordinates only.

Fig. 1. A table showing the test and trial spaces used by thermodynamic integration and the direct method, with respect to the weighted residuals described by Eq. (10).

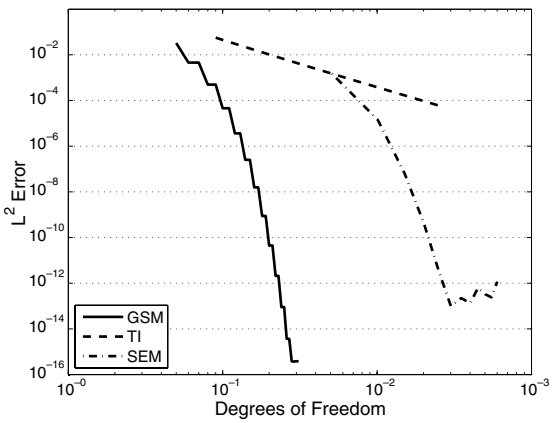

Fig. 2. Loglog plot of the L^2 error of solutions versus the degrees of freedom for the double well potential with the assumption of perfect sampling.

error resulting from using a small bin size. This is not to say that statistical error will no longer exist, it just won't be connected to bin size.

3.4.1. Multiple biased simulations

The method described by Eq. (11) assumes that samples are coming from an unbiased simulation. However, as discussed in Section 3.3, better sampling can be achieved by using several biased trajectories. To apply Eq. (11), the averages must be computed from a recombination of the biased trajectories. One possible way to do this is to use WHAM. Another approach requires a different choice for the weighting function $w(\zeta)$. Let u_k be the biasing potential for the kth of K biased trajectories. We will choose the weighting function

$$w(\zeta) = \sum_{k=1}^{K} \frac{\int \delta(\xi(x) - \zeta) \mathrm{e}^{-\beta(H(x,p)+u_k(\xi(x)))}\,\mathrm{d}x\,\mathrm{d}p}{\int \mathrm{e}^{-\beta(H(x,p)+u_k(\xi(x)))}\,\mathrm{d}x\,\mathrm{d}p}. \tag{14}$$

When substituted into Eq. (10) with trial functions ϕ_i and test functions ψ_j, this choice of weight function yields the system of equations

$$\sum_{i=1}^{N} A_i \sum_{k=1}^{K} \langle \phi_i'(\xi(x))\psi_j(\xi(x))\rangle^k = -\sum_{k=1}^{K} \langle F_\xi(x,p)\psi_j(\xi(x))\rangle^k \tag{15}$$

for $j = 1, \ldots, N$, where $\langle\cdot\rangle^k$ is the average coming from the kth biased trajectory. A derivation of Eq. (15) can be found in Section A.2. Notice that the components of the linear system produced by Eq. (15) are simple averages of the biased simulations. No explicit recombination step is necessary to compute the PMF using the weighted residual method.

4. Numerical experiments

To compare the methods for computing the PMF we performed a sequence of numerical experiments on two different systems. The first is the simple double well problem described in Section 3.4. The second is alanine dipeptide with the PMF computed along the ϕ dihedral angle. Two different error metrics were used to compare the quality of the approximation, $\widehat{A}$, with the exact PMF, A. These metrics measure the total error, the sum of the statistical and truncation error, made by the approximation. Recall that the PMF is defined up to an additive constant. We define the first metric to be the L^2 error minimized with respect to this constant

$$\|\widehat{A} - A\|_{L^2} = \min_{\alpha} \left(\int_a^b ((\widehat{A}(\zeta) + \alpha) - A(\zeta))^2\,\mathrm{d}\zeta \right)^{1/2}.$$

The second error metric, referred to as the difference error, measures the error in the change in free energy between two states. The difference error is defined at a pair of points on the interval of interest, $\zeta_1, \zeta_2 \in [a, b]$

$$|\widehat{A} - A|_D = |(\widehat{A}(\zeta_2) - \widehat{A}(\zeta_1)) - (A(\zeta_2) - A(\zeta_1))|.$$

The number of degrees of freedom (DOF) in the solution space used by TI, the direct method and WHAM is simply the number of elements or bins. For SEM and GSM the DOF is the number of coefficients used in the approximation to the PMF. To solve the WHAM equations, we used a fixed-point iteration with a tolerance of 10^{-3} using the method described in [21,22]. Further refinement did not have a significant effect on the results. To investigate both h and p-refinement, we applied the weighted residuals method using GSM and SEM. The basis functions for the global spectral method were constructed using

$$\phi_i(x) = \int_{\zeta_0}^{x} T_i\left(\frac{2x' - \zeta_f - \zeta_0}{\zeta_f - \zeta_0}\right) \mathrm{d}x',$$

where T_i is the *ith* Chebyshev polynomial and refinement is carried out only in p. In the figures, global spectral approximations are referred to as "GSM P", where P is the largest polynomial order used in the approximation. For SEM, we used a nodal basis on each element. Refinement was performed in both h and p. In the figures the approximations are referred to as "SEM E–P", where E is the number of elements and P is the polynomial order.

4.1. Double well PMF

For our first numerical experiment, we considered the simple double well system described in Section 3.4. The potential and corresponding PMF can be found in Eqs. (12) and (13). We used the reaction coordinate $\xi(x,y) = x$, on the interval $[-1.5, 1.5]$. A plot of the exact PMF can be seen in Fig. 3. Sampling was done using the Metropolis Monte Carlo algorithm described in [20], with $\beta = 2$, and an acceptance ratio of 35%. The simplicity of the two-dimensional configuration space made it possible to adequately sample the whole interval with a single unbiased simulation. When computing the difference error we used two critical points, $\zeta_l \approx -0.923$ and $\zeta_r = 0$, which correspond to the bottom and peak of one well.

The L^2 error as a function of the number of DOF is plotted in Fig. 4 with each plot corresponding to a different simulation length, 3.33×10^3 samples on the left and 3.33×10^5 samples on the right. Refinement for TI and the direct method is performed in h and both GSM and SEM refine in p. Notice in both plots the error of the direct method decreases until an optimal bin width is reached where statistical error is in balance with the truncation error, then increases as statistical error dominates. The remaining methods, all based on the weighted residual method, appear to level off for large degrees of freedom. For the plot with 3.33×10^5 samples, the global spectral method (denoted "GSM") initially achieves very rapid convergence similar to the

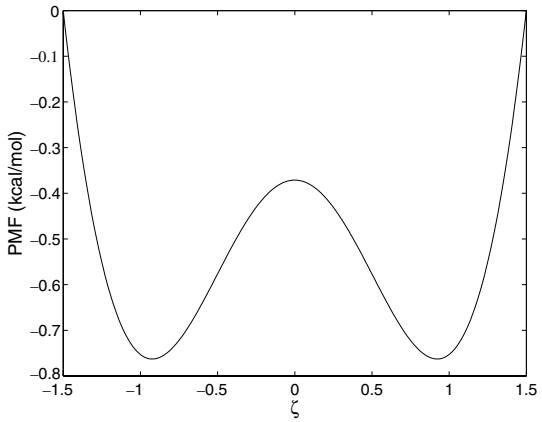

Fig. 3. Exact PMF for the potential from Eq. (12).

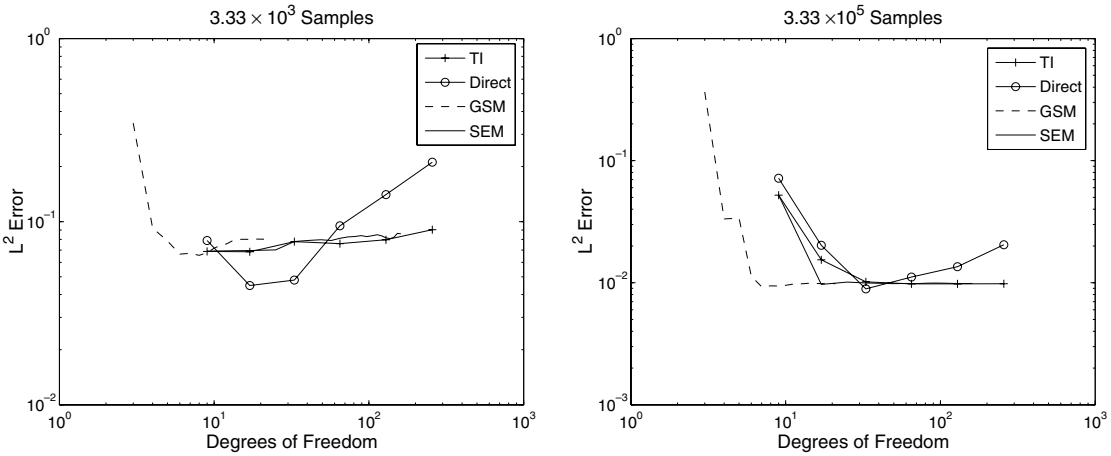

Fig. 4. Loglog plot of the L^2 error versus the DOF for the PMF of the double well potential in (12). Notice the direct method has a clear minimum after both 3.33×10^3 samples and 3.33×10^5 samples.

exponential convergence seen in Fig. 2. However, the curve levels when the statistical error begins to dominate. Also notice the direct method with optimal bin width achieves higher accuracy then the other methods for both numbers of samples. A similar pair of plots showing the difference error can be seen in Fig. 5. Again the direct method has a clearly optimal bin width. An interesting difference is that GSM has an error that is an order of magnitude less than the smallest error achieved by the remaining methods for fewer degrees of freedom.

Fig. 6 shows the L^2 and difference errors as functions of the number of samples for the four different methods. The TI and direct methods both have 50 degrees of freedom. The spectral element method (SEM) uses 12 elements with a cubic polynomial basis. Finally GSM is implemented with a degree 12 Chebyshev basis. The final line on the plots serves as a reference for $1/\sqrt{N}$, where N is the number of samples. The plot shows that all methods are converging in both norms as $1/\sqrt{N}$. In the L^2 plot all the methods have very similar error, the notable exception being the direct method. The direct method does not appear to do as well with the difference error over the entire length of the simulation. The remaining three methods again have very similar performance.

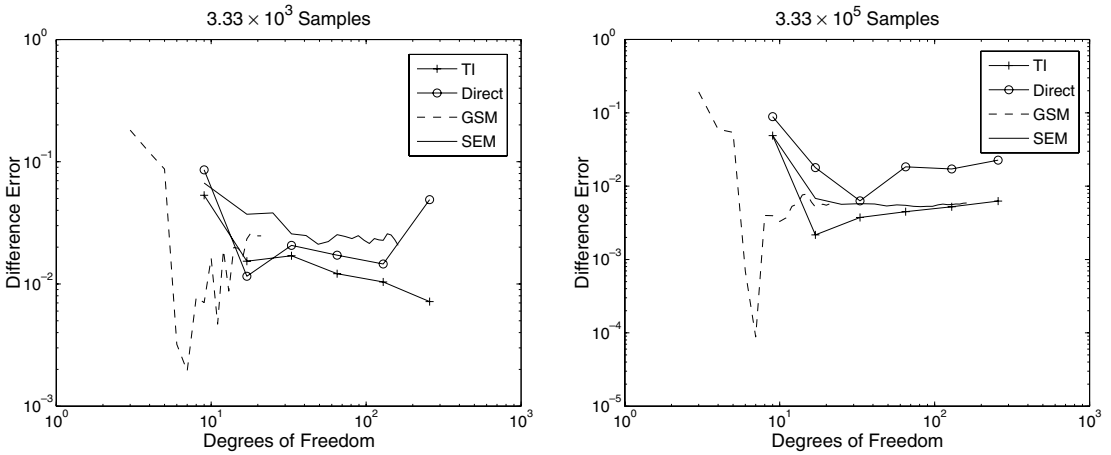

Fig. 5. Loglog plot of the difference error versus the DOF for the PMF of the double well potential in (12). On the left is the result after 3.33×10^3 samples, and on the right is after 3.33×10^5 samples.

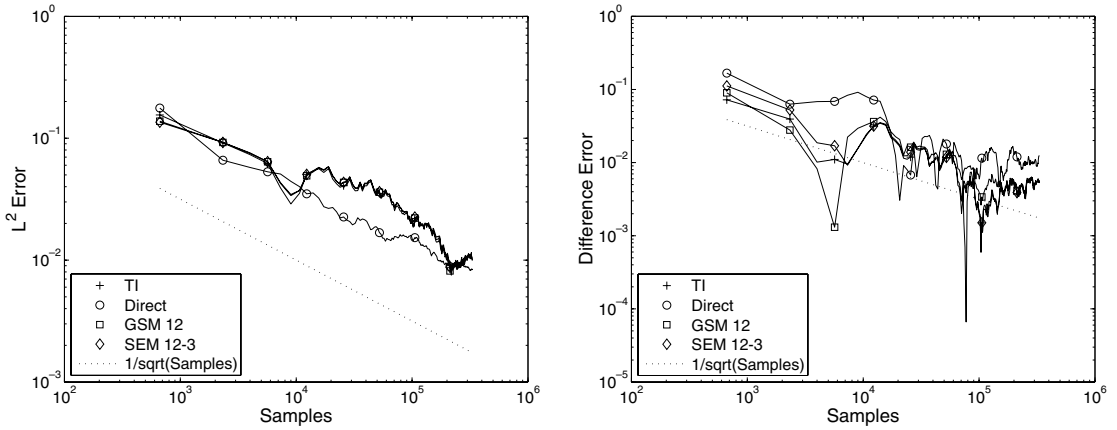

Fig. 6. L^2 error (on the left) and difference error (on the right) in the approximation to the PMF of the double well potential as a function of the number of samples.

4.2. Alanine dipeptide

To further examine the performance of the weighted residual methods a more realistic system was studied. Alanine dipeptide was chosen because it shares many of the characteristics of more complex biomolecules [25]. Furthermore, its small size reduces the computational effort required allowing for a more detailed comparison of numerical methods. All simulations were performed on a single workstation using the NAMD software program developed by the Theoretical and Computational Biophysics Group in the Beckman Institute for Advanced Science and Technology at the University of Illinois at Urbana-Champaign [26]. Each simulation generated configurations using Langevin dynamics in vacuum with 1 fs timesteps. The reaction coordinate under consideration was the ϕ dihedral angle measured in radians with $[-2.0, 1.5]$ being the interval of interest. The PMF from a 40 ns ABF simulation (shown in Fig. 7) was used as the "exact" PMF when calculating errors.

In the double well problem it was possible to sample the entire reaction coordinate using a single unbiased window. For this problem multiple windows had to be used. Initially, five evenly spaced overlapping windows of the same size were chosen to cover the reaction coordinate over the domain. This choice led to poor sampling surrounding the maxima of the PMF at $\phi \approx -0.13$. An additional window focusing sampling in this region fixed the problem. Sampling was constrained to each window by piecewise-quadratic biasing potentials of the form

$$u(\zeta) = \begin{cases} \frac{1}{2}c_l(\zeta - \zeta_l)^2 & \zeta < \zeta_l, \\ 0 & \zeta_l \leqslant \zeta \leqslant \zeta_r, \\ \frac{1}{2}c_r(\zeta - \zeta_r)^2 & \zeta_r < \zeta, \end{cases}$$

where c_l, c_r are coefficients controlling the strength of the restraint, and ζ_l, ζ_r are positions that define the size and placement of the window. A table listing the restraints and positions defining the six windows used can be seen in Fig. 8. Because of the use of multiple windows, WHAM was used instead of the direct method. Each window was run for a total of 2 ns or 2×10^6 time steps, yielding a total simulation time of 12 ns.

Fig. 9 shows the L_2 error as a function of DOF for different types of refinement. On the left is a snapshot after 0.75 ns of simulation and on the right is the full 12 ns of simulation. Both h and p refinement were investigated, using a static 8 elements for p-refinement (SEM-p) and cubic polynomials for h-refinement (SEM-h). Notice the error decreases with increased simulation time. In general the error is proportional to $1/\sqrt{t}$, where t is the length of the simulation. As with the double well potential, all the methods improve until the statistical error overwhelms the truncation error. Unlike the direct method for the double well potential, WHAM does not have an obvious optimal point where the statistical error balances with the truncation error. WHAM instead has a constant error for large numbers of degrees of freedom. The global spectral method again has very rapid convergence for small degrees of freedom, and is superior in the full 12 ns error calculation.

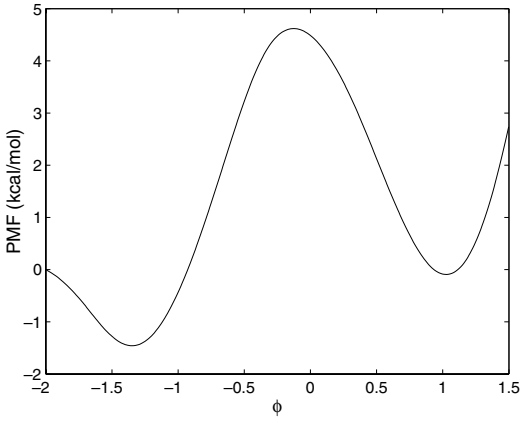

Fig. 7. PMF of alanine dipeptide in vacuum using the ϕ dihedral angle as the reaction coordinate, computed by a 40 ns ABF simulation.

	Win 1	Win 2	Win 3	Win 4	Win 5	Win 6
ζ_l	-2.0	-1.5	-0.8	-0.1	0.6	-0.4
ζ_r	-1.1	-0.4	0.3	1.0	1.5	0.4
c_l	60.0	60.0	60.0	60.0	60.0	30.0
c_r	60.0	60.0	60.0	60.0	60.0	30.0

Fig. 8. Windows used when computing the PMF for alanine dipeptide.

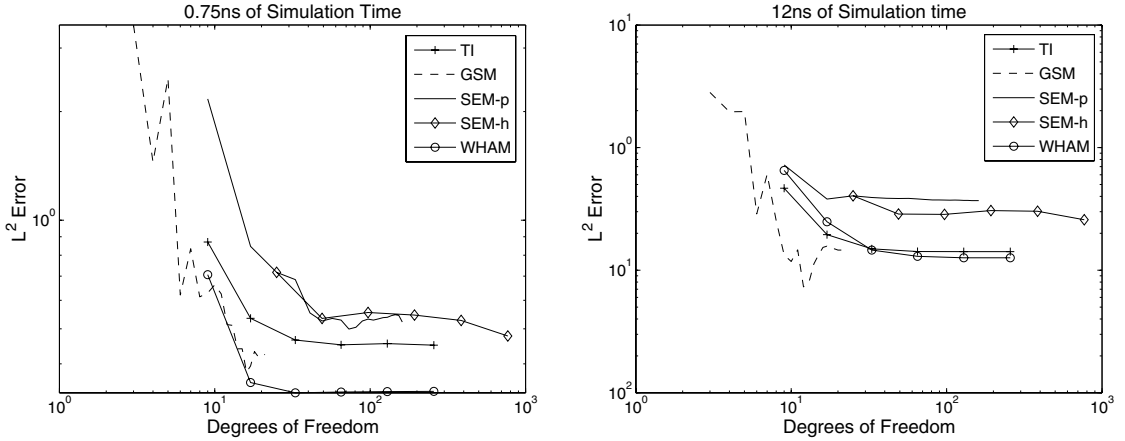

Fig. 9. Loglog plot of the L^2 error in the PMF for alanine dipeptide as a function of the DOF for 0.75 ns (on the left) and 12 ns (on the right) of total simulation time.

Fig. 10 is similar to Fig. 9 but uses the difference error defined at the points $\phi = -0.13$ and $\phi = 1.03$. Using this error metric both the h and p-refined SEM methods perform better than suggested by the L^2 metric. Though the global spectral method is still superior for the total simulation time of 12 ns.

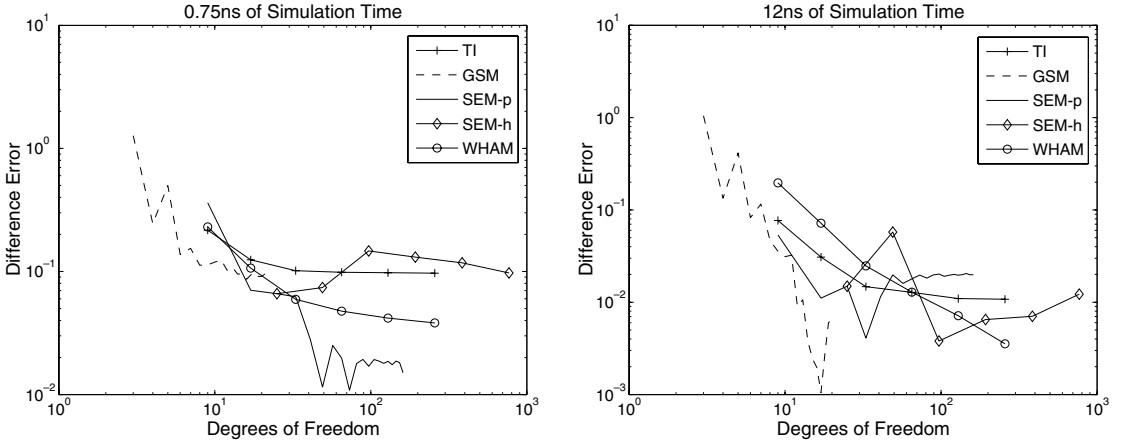

Fig. 10. Loglog plot of the difference error in the PMF for alanine dipeptide as a function of the DOF for 0.75 ns (on the left) and 12 ns (on the right) of total simulation time.

5. Conclusion

We have developed a framework based on the method of weighted residuals for approximating the potential of mean force (PMF) along a reaction coordinate. This framework is general enough to encompass thermodynamic integration and direct histogram methods, providing an analysis tool for comparing the two. In addition, using weighted residuals allows for higher-order approximations to the PMF in the form of a global spectral method or a spectral element method. When implemented, the result is a linear system of equations for determining the unknown PMF from ensemble averages generated by equilibrium molecular dynamics or Monte Carlo simulations. We have shown that this holds true even when multiple biased trajectories are used. In our analysis, we have demonstrated that higher-order methods allow for exponential convergence through p-refinement when configurational space is sampled sufficiently well. For fewer samples statistical error dominates and is governed by the law of large numbers, which is proportional to $1/\sqrt{N}$, where N is the number of samples. In numerical experiments involving a double-well potential and alanine dipeptide, we have shown that the global spectral method is remarkably robust as the polynomial degree is increased. When the sampling rate was high and the polynomial degree was low, the global spectral method retained its exponential convergence rate. As the polynomial degree was increased and statistical error dominated, the total accuracy remained nearly constant. This is in contrast to histogram methods which suffer from increased statistical error as the bin size is refined. Finally, the higher degree of continuity provided by spectral methods makes weighted residuals an attractive choice for use in conjunction with biasing force methods.

Acknowledgments

The authors would like to thank Prof. Robert Skeel for many helpful and stimulating discussions, and the reviewers for their insightful comments.

Appendix A

A.1. Direct methods as weighted residuals

In this section reaction coordinates will have two classifications, first aperiodic reaction coordinates which assumes that at some ζ_0 and ζ_f, with $\zeta_0 < \zeta_f$, the system is restrained, i.e. $\rho_\xi(\zeta_0) = \rho_\xi(\zeta_f) = 0$. Notice that this includes infinite reaction coordinates. The second classification is a periodic reaction coordinate, which is defined by $\zeta_0 = \zeta_f$ and $\rho_\xi(\zeta_0) = \rho_\xi(\zeta_f)$.

A.1.1. Aperiodic reaction coordinate

First consider the weighted residual method defined by Eq. (10). Using $\rho_\xi(\zeta) = \mathrm{e}^{-\beta A(\zeta)}$, notice

$$-\beta\rho_\xi(\zeta)\left(\frac{\mathrm{d}A}{\mathrm{d}\zeta} + \langle F_\xi\rangle_\zeta\right) = \frac{\mathrm{d}}{\mathrm{d}\zeta}[\rho_\xi(\zeta)] - \beta\overline{F}_\xi(\zeta).$$

Multiplying Eq. (10) by $-\beta$ and substituting the above expression gives the set of N equations

$$\int_{\zeta_0}^{\zeta_f}\left(\frac{\mathrm{d}}{\mathrm{d}\zeta}[\rho_\xi(\zeta)] - \beta\overline{F}_\xi(\zeta)\right)\psi_j(\zeta)\,\mathrm{d}\zeta = 0 \quad \text{for } j = 1,\ldots,N.$$

Now approximate $\rho_\xi(\zeta)$ as a linear combination of the trial functions $\{\phi_i\}_{i=1}^N$. Substituting in the approximation gives the linear system

$$\sum_{i=1}^{N} P_i \int_{\zeta_0}^{\zeta_f} \phi_i'(\zeta)\psi_j(\zeta)\,\mathrm{d}\zeta = \int_{\zeta_0}^{\zeta_f} \beta\overline{F}_\xi(\zeta)\psi_j(\zeta)\mathrm{d}\zeta \quad \text{for } j = 1,\ldots,N.$$

After first substituting $\beta\overline{F}_\xi(\zeta) = \frac{\mathrm{d}}{\mathrm{d}\zeta}[\rho_\xi(\zeta)]$ and then integrating by parts on both sides we find

$$\sum_{i=1}^{N} P_i\left[(\phi_i(\zeta)\psi_j(\zeta)|_{\zeta_0}^{\zeta_f} - \int_{\zeta_0}^{\zeta_f}\phi_i(\zeta)\psi_j'(\zeta)\,\mathrm{d}\zeta\right] = -\int_{\zeta_0}^{\zeta_f}\rho_\xi(\zeta)\psi_j'(\zeta)\,\mathrm{d}\zeta \quad \text{for } j = 1,\ldots,N, \tag{A.1}$$

where the boundary terms vanish on the right-hand-side because of the assumption that the reaction coordinate is restrained ($\rho_\xi(\zeta_0) = \rho_\xi(\zeta_f) = 0$).

Choose a set of Δ spaced grid points on the interval (ζ_0, ζ_f), where $\zeta_1 > \zeta_0 + \Delta/2$ and $\zeta_N < \zeta_f - \Delta/2$. The objective is to approximate $\rho_\xi(\zeta)$ on this grid, to this end we will use as trial functions the basis $\phi_i(\zeta)$ for $i = 1, \ldots, N$, where

$$\phi_i(\zeta) = \begin{cases} 1 & \zeta_i - \Delta/2 \leqslant \zeta \leqslant \zeta_i + \Delta/2, \\ 0 & \text{otherwise.} \end{cases} \tag{A.2}$$

The choice of grid points and basis functions enforces that the piecewise-constant approximation to $\rho_\xi(\zeta)$ will be zero at ζ_0 and ζ_f. If we require that a function ψ_i in the test space satisfies $\psi_i'(\zeta) = \phi_i(\zeta)$ and substitute the definitions of ϕ_i and ψ_j into Eq. (A.1) we find

$$P_j = \frac{1}{\Delta} \int_{-\Delta/2}^{\Delta/2} \rho_\xi(\zeta_j + \zeta) \mathrm{d}\zeta \quad \text{for } j = 1, \ldots, N.$$

Therefore the coefficients of P_i as calculated by this weighted residual method are equivalent to the coefficients calculated by the direct method (see Eq. (6)). Since the trial space is piecewise-constant, the direct method is the same as applying the weighted residuals method defined by Eq. (10) with the same trial space, and a piecewise-linear test space.

A.1.2. Periodic reaction coordinate

Define the points $\zeta_0 = \zeta_1, \ldots, \zeta_N = \zeta_f$ and use $\phi_i(\zeta)$ from Eq. (A.2) for $i = 2, \ldots, N-1$. For $i = 1$ define ϕ_i as

$$\phi_1(\zeta) = \begin{cases} 1 & \zeta_1 \leqslant \zeta \leqslant \zeta_1 + \Delta/2, \\ 1 & \zeta_N - \Delta/2 \leqslant \zeta \leqslant \zeta_N, \\ 0 & \text{otherwise.} \end{cases}$$

Notice that for $i = 1, \ldots, N-1$ the functions $\phi_i(\zeta)$ are periodic on $[\zeta_0, \zeta_f]$. Now assume that $\psi_j(\zeta)$ for $j = 1, \ldots, N-1$ are periodic test functions. Repeating the same steps for the weighted residual method as above in the aperiodic reaction coordinate example gives

$$\sum_{i=1}^{N-1} P_i \left[(\phi_i(\zeta)\psi_j(\zeta)|_{\zeta_0}^{\zeta_f} - \int_{\zeta_0}^{\zeta_f} \phi_i(\zeta)\psi_j'(\zeta)\,\mathrm{d}\zeta \right] = \left[(\rho_\xi(\zeta)\psi_j(\zeta)|_{\zeta_0}^{\zeta_f} - \int_{\zeta_0}^{\zeta_f} \rho_\xi(\zeta)\psi_j'(\zeta)\,\mathrm{d}\zeta \right].$$

Using the periodicity of $\phi_i(\zeta)$, $\psi_j(\zeta)$, $\rho_\xi(\zeta)$ and applying the definition of $\phi_i(\zeta)$ yields

$$\sum_{i=1}^{N-1} P_i \int_{-\Delta/2}^{\Delta/2} \psi_j'(\zeta_i + \zeta)\,\mathrm{d}\zeta = \int_{\zeta_0}^{\zeta_f} \rho_\xi(\zeta)\psi_j'(\zeta)\,\mathrm{d}\zeta.$$

Now let $\psi_j'(\zeta) = \phi_j(\zeta)$. For $\psi_j(\zeta)$ to be periodic it has to be 0 everywhere but on the interval $[\zeta_j - \Delta/2, \zeta_j + \Delta/2]$ where the function is linear from $\psi_j(\zeta_j - \Delta/2) = 0$ to $\psi_j(\zeta_j + \Delta/2) = \Delta$. The specific form is

$$\psi_j(\zeta) = \begin{cases} 0 & \zeta < \zeta_j - \Delta/2, \\ \zeta - (\zeta_j - \Delta/2) & \zeta_j - \Delta/2 \leqslant \zeta \leqslant \zeta_j + \Delta/2, \\ 0 & \zeta > \zeta_j + \Delta/2. \end{cases}$$

This set of test functions, $\psi_j(\zeta)$ for $j = 1, \ldots, N-1$ gives the same values computed by the direct method for the coefficients P_j.

A.2. Biased weighted residuals

The weight function in Eq. (14) can also be written as

$$w(\zeta) = \rho_\xi(\zeta) \sum_{k=1}^{K} \frac{e^{-\beta u_k(\zeta)}}{\langle e^{-\beta u_k} \rangle}.$$

Using trial functions ϕ_i and test functions ψ_j, and substituting $w(\zeta)$ into Eq. (10) yields

$$\sum_{i=1}^{N} A_i \sum_{k=1}^{K} \frac{\int \phi_i'(\xi(x))\psi_j(\xi(x))e^{-\beta(H(x,p)+u_k(\xi(x)))}\,dx\,dp}{\int e^{-\beta(H(x,p)+u_k(\xi(x)))}\,dx\,dp} = -\sum_{k=1}^{K} \int \langle F_\xi \rangle_\zeta \psi_j(\zeta)\rho_\xi(\zeta)\frac{e^{-\beta u_k(\zeta)}}{\langle e^{-\beta u_k} \rangle}\,d\zeta$$

for $j = 1, \ldots, N$. Applying Eq. (5), the right-hand-side can be further simplified

$$\begin{aligned}\sum_{k=1}^{K} \int \langle F_\xi \rangle_\zeta \psi_j(\zeta)\rho_\xi(\zeta)\frac{e^{-\beta u_k(\zeta)}}{\langle e^{-\beta u_k} \rangle}\,d\zeta &= \sum_{k=1}^{K} \int \overline{F}_\xi(\zeta)\psi_j(\zeta)\frac{e^{-\beta u_k(\zeta)}}{\langle e^{-\beta u_k} \rangle}\,d\zeta \\ &= \sum_{k=1}^{K} \frac{\int F_\xi(x,p)\psi_j(\xi(x))e^{-\beta(H(x,p)+u_k(\xi(x)))}\,dx\,dp}{\int e^{-\beta(H(x,p)+u_k(\xi(x)))}\,dx\,dp}.\end{aligned}$$

Notice that both sides are composed of sums of biased trajectory averages. This gives the simple form

$$\sum_{i=1}^{N} A_i \sum_{k=1}^{K} \langle \phi_i'(\xi(x))\psi_j(\xi(x)) \rangle^k = -\sum_{k=1}^{K} \langle F_\xi(x,p)\psi_j(\xi(x)) \rangle^k \quad \text{for } j = 1, \ldots, N,$$

where $\langle \cdot \rangle^k$ is the average from the kth biased trajectory.

References

[1] P. Kollman, Free energy calculations: applications to chemical and biochemical phenomena, Chem. Rev. 93 (1993) 2395–2417.
[2] J.G. Kirkwood, Statistical mechanics of fluid mixtures, J. Chem. Phys. 3 (1935) 300–313.
[3] D. Chandler, Statistical mechanics of isomerization dynamics in liquids and the transition state approximation, J. Chem. Phys. 68 (1978) 2959–2970.
[4] G.M. Torrie, J.P. Valleau, Nonphysical sampling distributions in Monte Carlo free-energy estimation : umbrella sampling, J. Comput. Phys. 23 (1977) 187–199.
[5] S. Kumar, D. Bouzida, R.H. Swendsen, P.A. Kollman, J.M. Rosenberg, The weighted histogram analysis method for free-energy calculations on biomolecules. I. The method, J. Comput. Chem. 13 (8) (1992) 1011–1021.
[6] R.W. Zwanzig, High-temperature equation of state by a perturbation method. I. Nonpolar gases, J. Chem. Phys. 22 (1954) 1420–1426.
[7] M. Mezei, D.L. Beveridge, Free energy simulations, Ann. NY Acad. Sci. USA 482 (1986) 1–23.
[8] M.R. Mruzik, F.F. Abraham, D.E. Schreiber, G.M. Pound, A Monte Carlo study of ion–water clusters, J. Chem. Phys. 64 (1976) 481–491.
[9] S. Park, K. Schulten, Calculating potentials of mean force from steered molecular dynamics simulations, J. Chem. Phys. 120 (2004) 5946–5961.
[10] E. Darve, A. Pohorille, Calculating free energies using average force, J. Chem. Phys. 115 (20) (2001) 9169–9183.
[11] E. Darve, M.A. Wilson, A. Pohorille, Calculating free energies using a scaled-force molecular dynamics algorithm, Mol. Simul. 28 (2002) 113–144.
[12] D. Rodriguez-Gomez, E. Darve, A. Pohorille, Assessing the efficiency of free energy calculation methods, J. Chem. Phys. 120 (2004) 3563–3578.
[13] J. Hénin, C. Chipot, Overcoming free energy barriers using unconstrained molecular dynamics simulations, J. Chem. Phys. 121 (7) (2004) 2904–2914.
[14] T.P. Straatsma, J.A. McCammon, Multiconfiguration thermodynamic integration, J. Chem. Phys. 95 (1991) 1175–1188.
[15] C. Chipot, P.A. Kollman, D.A. Pearlman, Alternative approaches to potential of mean force calculations: free energy perturbation versus thermodynamic integration. Case study of some representative nonpolar interactions, J. Comput. Chem. 17 (9) (1996) 1112–1131.
[16] R.J. Radmer, P.A. Kollman, Free energy calculation methods: a theoretical and empirical comparison of numerical errors and a new method for qualitative estimates of free energy changes, J. Comput. Chem. 18 (1997) 902–919.
[17] W.K. den Otter, Thermodynamic integration of the free energy along a reaction coordinate in Cartesian coordinates, J. Chem. Phys. 112 (17) (2000) 7283–7292.
[18] M.N. Kobrak, Systematic and statistical error in histogram-based free energy calculations, J. Comput. Chem. 24 (2003) 1437–1446.
[19] D.A. Pearlman, Determining the contributions of constraints in free energy calculations: development, characterization, and recommendations, J. Chem. Phys. 98 (11) (1993) 8946–8957.
[20] D. Frenkel, B. Smit, Understanding Molecular Simulation, second ed., Academic Press, 2001.
[21] B. Roux, The calculation of the potential of mean force using computer simulations, Comput. Phys. Commun. 91 (1995) 275–282.

[22] M. Souaille, B. Roux, Extension to the weighted histogram analysis method: combining umbrella sampling with free energy calculations, Comput. Phys. Commun. 135 (2001) 40–57.
[23] G.E. Karniadakis, S. Sherwin, Spectral/hp Element Methods for Computational Fluid Dynamics, second ed., Oxford University Press, 2005.
[24] John P. Boyd, Chebyshev and Fourier Spectral Methods, second ed., Dover, 2001.
[25] P.G. Bolhuis, C. Dellago, D. Chandler, Reaction coordinates of biomolecular isomerization, Proc. Natl. Acad. Sci. USA 97 (11) (2000) 5877–5882.
[26] J.C. Phillips, R. Braun, W. Wang, J. Gumbart, E. Tajkhorshid, E. Villa, C. Chipot, R.D. Skeel, L. Kale, K. Schulten, Scalable molecular dynamics with NAMD, J. Comput. Chem. 26 (2005) 1781–1802.